Fast-quenched $Na_2Si_2O_5$ stability and properties in crystalline composite

Smeacetto, F.; Saffirio, S.; Salvo, M.; Palliotto, A.; Zhang, J.; De Angelis, S.; Tinti, V.B.; Esposito, V.

Published in:
Materialia

Link to article, DOI:
10.1016/j.mtla.2023.101968

Publication date:
2024

Document Version
Publisher's PDF, also known as Version of record

MTLA 33 (2024) 101968

Contents lists available at ScienceDirect

Materialia

journal homepage: www.elsevier.com/locate/mtla

Fast-quenched $Na_2Si_2O_5$ stability and properties in crystalline composite

F. Smeacetto [a,*], S. Saffirio [a], M. Salvo [a], A. Palliotto [a,b], J. Zhang [b,1], S. De Angelis [b], V.B. Tinti [b], V. Esposito [b,*]

[a] Department of Applied Science and Technology (DISAT), Politecnico di Torino, C.so Duca degli Abruzzi 24, Torino 10129, Italy
[b] Department of Energy Conversion and Storage, Technical University of Denmark, Kgs. Lyngby 2800, Denmark

ARTICLE INFO

Keywords:
Na-ionic conductivity
Glass ceramics
Mass diffusion
Sodium ionic glass conductors

ABSTRACT

The sinter-crystallisation method of as-casted glass-based materials is effective for obtaining glass ceramics with different functional properties. We here report the microstructural, chemical composition, and ion dynamics of a fast Na-ion conductor $Na_2Si_2O_5$ synthesised by the melt-quenching route. The parent glass is treated under different temperatures and crystallisation times. The analysis shows that the electrical properties strongly depend on the material's microstructural properties and thermal history. The fast-quenched materials achieve greater stability and electrical properties, outperforming the solid-state reaction methods and $SrSiO_3$—$Na_2Si_2O_5$ composites. We show that the crystalline regions in the sintered material act as nucleation centres for the recrystallised $Na_2Si_2O_5$ phase, affecting the conductivity. The melt-quenched material shows a high conductivity of 10^{-1} S cm^{-1} at 750 °C. Furthermore, the recrystallisation process of $Na_2Si_2O_5$ is reversible, leading to a *facile* regeneration of the ionic properties.

1. Introduction

Solid-state ionic sodium conductors are key functional materials for battery technology. For this application, an inorganic solid electrolyte prevents explosions and leakage. It improves battery safety and is less toxic than organic liquid electrolytes [1,2]. Furthermore, a solid-state electrolyte allows new and different electrodes to increase the cell's energy density [3]. Inorganic solid electrolytes have shown promising conductivity values, enabling a possible application as an All-Solid-State electrolyte for batteries. NASICON-Type $Na_3Zr_2Si_2PO_{12}$, β-Alumina and sulfide electrolytes are among the most interesting materials with sodium conductivities of over 10^{-3} S cm^{-1} [4–6].

An attractive alternative for intermediate temperatures sodium conductors is sodium-strontium silicate ($Sr_{3-3x}Na_{3x}Si_3O_{9-1.5x}$, SNS). Goodenough et al. discovered these materials and were originally classified as fast oxygen-ion conductors for low-temperature solid oxide fuel cells (IT-SOFCs) [7,14]. However, subsequent studies clearly showed the pure Na-conductivity properties ranging from 10^{-5} to 10^{-3} S cm^{-1} in the RT-600 C range [15–17]. SNS electrical properties are limited to a temperature of around 600 °C due to a recrystallisation process of $Na_2Si_2O_5$ (RC—NS) [15,17]. Evans et al. have shown, through powder neutron diffraction, that only a low amount of Na-doped $SrSiO_3$ is present, and the conductivity of the samples increased with increasing content of amorphous-Na_2SiO_5 (am-NS) [9]. Phase transformations in the SNS ($x = 0.45$) system have also been investigated through NMR spectroscopy, confirming the sodium transport [9–12]. Bayliss et al. also showed through a DFT calculation that the formation of oxygen vacancies is less likely to occur, and if they were present, they would not cause high conductivities [8,13]. Later, it was demonstrated that SNS is a two-phase system composed of $Na_2Si_2O_5$ (NS) and $SrSiO_3$ (SS). EDX analysis on an SNS composite ($x = 0.45$) showed the presence of two phases, one with a chemical composition of Na: Si ≈ 1: 1 with a low concentration of Sr. On the contrary, the other phase showed a similar ratio in Sr: Si. These results suggest a phase separation of $Sr_{3-3x}Na_{3x}Si_3O_{9-1.5x}$ into NS and SS [16]. Furthermore, it was shown that amorphous NS had higher conductivities than any other SNS composition. However, NS in SNS, if produced with a solid-state reaction technique, is thermally unstable at high temperatures (> 600 °C), and it recrystallises into an insulating phase, *i.e.*, the RC—NS phase [16,17]. Such instability can be linked to the synthetic method used, leading to important differences in the final properties of the material [24,25]. Crystalline SS in *heat-treated* materials, *i.e.* with an uncontrolled thermal history, can thus cause early and faster nucleation of the amorphous phase, causing a lower temperature stability window. On the other

* Corresponding authors.
E-mail addresses: federico.smeacetto@polito.it (F. Smeacetto), vies@dtu.dk (V. Esposito).
[1] This author equally contributed to this work.

https://doi.org/10.1016/j.mtla.2023.101968
Received 31 May 2023; Accepted 22 November 2023
Available online 28 November 2023

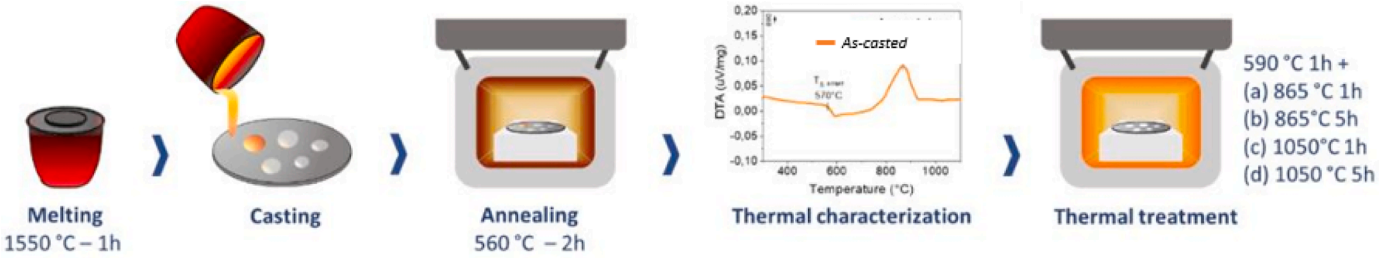

Fig. 1. Schematic of the methodology and results, including the DTA curve of the as-casted SNS bulk glass showing its characteristic glass transition (Tg – 570 °C) and peak crystallisation (T_p – 865 °C) temperatures.

hand, high Na-ion conductivity materials, stable at intermediate temperatures, enable the development of intermediate-temperature Na-ion all-solid-state batteries or can be used in other applications that require intermediate-temperature stability. NS and SNS are good candidates for these applications since they show chemical stability, low toxicity and cost. The conductivities decreased with increasing strontium silicate (SS) content, and NS showed the highest conductivities. Jee et al. produced an amorphous NS sample, which showed a conductivity drop at a lower temperature (500 °C) due to the early nucleation of RC—NS [17].

Since the amorphous NS is responsible for the conduction mechanism in the material, we use a melt-quenching route to produce an amorphous NS glass in place of the commonly used *heat-treated* materials by the solid-state reaction technique. Yet, fast-quenching allows greater and simpler industrialisation due to the facile fabrication, which does not involve high pressures [17]. Phosphate glasses and glass ceramics have been extensively studied in recent decades, showing higher conductivities and wider temperature range stability [27]. We here delay NS recrystallisation through this process and avoid an early conductivity drop. Thus, we can exploit the higher conductivities of NS at higher temperatures (> 500 °C). We also compare the conductivity of NS and SNS to understand the effect of crystalline strontium silicate on the RC—NS nucleation and sodium conduction; SS is a crystalline phase that can enhance the crystallisation of NS since it can act as a nucleation centre.

Moreover, melt-quenching and successive post-treatments allow controlling microstructural evolution in SNS with a potentially wider spectrum of crystal sizes while optimising ionic conductivity. The SNS ($x = 0.45$) is selected as the most studied composition. We investigate the effect of this never-before-used production technique to manufacture NS glass and its composites. To comprehend how to expand the stability temperature range of am-NS, we analyse the impact of a crystalline phase in the nucleation process of RC—NS. By studying SNS, we also investigate the benefits and drawbacks of using an insulating crystalline phase (SS).

2. Materials and methods

2.1. Synthesis of the SNS glass-ceramic system

The SNS parent glass was produced using conventional melting and casting from the following high-purity grade raw materials: $SrCO_3$ (EMSURE ACS, 99.0 %), Na_2CO_3 (Alfa Aesar, 99.9 %), and SiO_2 (Aldrich, 99.99 %) for the preparation of the glass-ceramic system with a composition consisting in 31SrO-12.7Na_2O-56.3SiO_2 (mol.%), labelled as SNS. Fig. 1 shows schematically the process.

The precursors were thoroughly mixed for 24 h, transferred into a Pt crucible, and then placed into an electric furnace at 1550 °C for 1 h to decompose carbonates and form a homogeneous melt. The resulting SNS glass was cast onto a heated brass plate (*as-casted* sample) and immediately transferred into a furnace at 560 °C (10 °C below the glass-transition temperature, T_g) for 2 h for an annealing treatment. After that, according to the thermal characterisation carried out on the *as-casted* glass, bulk materials were devitrified and thus transformed into glass ceramics, hereafter referred to as *heat-treated* samples, through different thermal treatments (Fig. 1).

Each treatment consisted of a first step at 20 °C above the T_g for 1 h to induce the nucleation of crystalline grains, followed by a high-temperature step at 865 °C, 1 or 5 h or 1050 °C 1 or 5 h to allow for the growth of the crystalline phase. Part of the *as-casted* glass was not devitrified but instead milled for 2 h into a Zirconia grinding bowl and sieved below 25 μm. This procedure was carried out to compare the devitrification of the bulk system with the sintering of its powders counterpart (referred to as *pellet SNS*). According to their thermal-mechanical properties (see thermal characterisation), SNS glass powders were sintered at 800 °C for 1 h.

The same melt-casting procedure produced the individual bulk NS and SS systems (single phases) to investigate the thermal and ion-conducting behaviour of the SNS system's two phases. Specifically, NS was held at 1350 °C before casting and SS at 1650 °C for 1 h. Both glasses were immediately transferred for 2 h into a furnace at 10 °C lower than their glass-transition temperature to release thermal stresses.

2.2. Characterisation techniques

Differential thermal analysis (DTA, Netzsch, DTA 404 PC) was carried out in *quasi*-static air on SNS as-casted glass in the form of bulk and powder material to evaluate their glass transition (T_g) and peak crystallisation (T_p) temperatures. In particular, DTA on the bulk and powder as-casted glass was performed in the temperature range between 25 (RT) and 1100 °C at a heating rate of 10 °C min^{-1} in air. The heat treatments performed to devitrify the bulk glasses into glass ceramics (SNS *heat-treated* samples) were defined accordingly, as well as for the solid-state sintering of the SNS glass powders. Further DTA analyses were carried out on bulk glass-ceramic samples to investigate their thermal behaviour under cyclic heating and cooling conditions. In particular, samples were subjected to the first heating step up to 800 °C, then by cooling down to RT (room temperature) and then to a second heating ramp up to 1050 °C again, then by cooling down to RT. Each step of cyclic DTA was performed at the heating rate of 10 °C min^{-1}. Linear DTA from RT up to 1100 °C was also carried out on the bulk *as-casted* samples to assess their thermal behaviour upon continuous heating. Linear DSC from RT up to 1100 °C at a scan rate of 10 °C min^{-1} in air was carried out on the bulk NS and SS separate systems.

Crystalline phases were identified by X-ray diffraction analysis (XRD, Panalytical, Xpert3 MRD) at RT using Cu Kα radiation at 40 kV and a current of 40 mA. The XRD patterns were recorded in the 2θ range of 10–70° on both *as-casted* and *heat-treated* to follow the transformation of each phase. XRD measurements were conducted with *in-situ* heating under an inert atmosphere (N_2, 99.999 %). The samples were heated and cooled at 5 °C/min from room temperature to 1050 °C with a stabilisation time of 10 mins before each acquisition. The XRD patterns were further analysed using the Rietveld Refinement method [18]. For that, the software TOPAS-Academic v.8 [19] was employed to make a sequential type of refinement. Sequential refinement was conducted

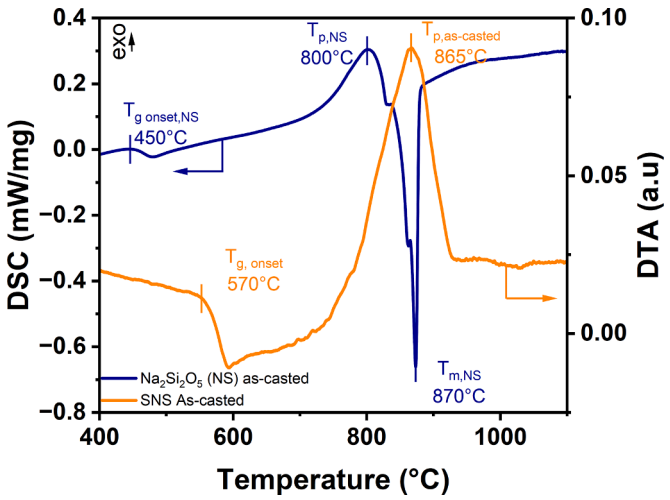

Fig. 2. DTA and DSC results on bulk NS and SNS *as-casted*.

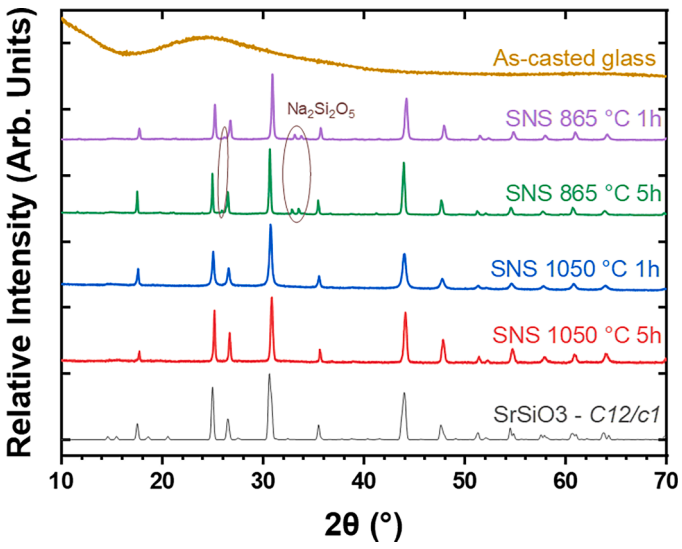

Fig. 3. XRD characterisation at room temperature of SNS *as-casted* and thermally treated at 865 °C and 1050 °C for 1 and 5 h. The patterns do not show any peak diffractions for the *as-casted* glass. After thermal treatment, the samples show the presence of the $SrSiO_3$ (*SS*) phase.

using the obtained refined values of a previous temperature as starting values for the next [20], following the measurement order. In total, 43 different diffraction patterns were comprised in the sequential setup. The measured XRD were compared with the ICSD patterns [21,22,26].

Microstructures were observed using scanning electron microscopy (SEM, JEOl, JCM-6000Plus, BenchtopSEM) on the polished surfaces of the samples under high vacuum and an acceleration voltage of 15 kV. Elemental analysis was performed through energy-dispersive X-ray spectroscopy (EDS, Jeol, EX-37,001) in the same operating conditions.

Electrochemical Impedance Spectroscopy was used to study the electrical properties of the materials. For the measurements, we have used two different kinds of electrodes, especially to clarify the effect of the thermal treatment on the electrical properties:

1. Pt-electrodes: Pt paste was brushed on both sides of the SNS *heat-treated* sample and then heat-treated at 900 °C, *i.e.* above the Tg, for 2 h.
2. Ag-electrodes: a silver paste for all the samples. The paste is conductive at RT and keeps conducting up to high temperatures. It was hand-brushed on both sides and used for the EIS measurements. The measurements with silver electrodes were carried out to replace the Pt-electrodes samples and the *as-casted, pellet, bulk* and *heat-treated* samples with no further curing treatments.

Two *pellet* and two *heat-treated* SNS samples were tested, one in synthetic air and the other in reducing conditions, *i.e.* in a 3 % H_2/Ar atmosphere. The electrochemical impedance spectra (EIS) were collected with 10 mV AC amplitude ranging from 1 MHz to 0.6 Hz using a Solartron 1260 frequency response analyser. Thermal cycling was performed on the SNS samples (*pellet* and *heat-treated*) from room temperature to 800 °C and back ten times with a temperature step of 50 °C. The electrodes for the bulk NS and SS samples were prepared by hand-brushing Ag silver paste on both sides to act as counter and working electrodes, *i.e.* symmetric cell configuration. The EIS spectra for these two samples were collected in four thermal cycles (heating and cooling), the first two from RT to 500 °C— instead, the last two from RT to 750 °C, with a 50 °C temperature step. The first two temperature scans were added to check the stability of the am-NS in this temperature range.

3. Results and discussion

A series of different heat treatments, in terms of times and temperatures, were tailored for the bulk system. The thermal analysis on *as-casted* SNS and NS systems (Fig. 2) shows that T_g is around 570 °C and 450 °C, respectively.

The NS *as-casted* sample showed a crystallisation peak at 800 °C and a melting behaviour at 870 °C, thus showing its tendency to devitrification. In comparison, one exothermic peak (corresponding to the formation of a crystalline phase) is present at 865 °C for the SNS *as-casted* sample, indicating its maximum crystallisation rate. A first nucleation step of 1 hour at a temperature of 20 °C above the T_g (590 °C) was set for all samples, followed by a dwelling at 865 °C or 1050 °C for 1 or 5 h to allow for grain growth. The crystallisation of the bulk samples was carried out at two different temperatures:

1. 865 °C, corresponding to the maximum crystallisation rate resulting from DTA,
2. 1050 °C, in agreement with the earliest study by Goodenough et al. [7], where the authors carried out the sintering of Sr3-xA3xSiO9–1.5x (*A* = K or Na) powders through a solid-state reaction at 1000 °C and 1050 °C for 20 h.

The XRD analysis shows the glass-to-SNS transition in the heat-treated samples (Fig. 3). The *as-casted* glass material exhibits an amorphous structure. At the same time, the appearance of the SS phase occurs after thermal treatment according to the specified conditions, *i.e.*, dwelling at 865 °C (to achieve the maximum crystallisation rate) or at 1050 °C for durations of 1 or 5 h. A characteristic diffraction pattern displaying an amorphous broad range is observed for the as-casted SNS glass. Conversely, the principal SS crystalline phase (JCPDS reference code: 00–034–0099, with major reflections at 30.6°, 43.9°, and 24.9°) is discernible in all *heat-treated* samples. The corresponding reference diffraction pattern of this SS crystalline phase is depicted in Fig. 8.

Of particular note, three additional peaks at 26.2°, 33.1°, and 33.7° become apparent in samples treated at 865 °C, signifying the presence of an additional crystalline phase. These peaks are attributed to the NS phase and are absent in samples treated up to 1050 °C. The dynamic processes encompassing the formation, transformation, and eventual vanishing of this phase as temperature increases, alongside its consequential impact on the ionic conductivity across the broader SNS system, are presented and comprehensively deliberated in subsequent DSC, EIS, and in-situ XRD characterisations.

Microstructures of the glass-ceramics obtained with the four thermal treatments mentioned above are shown in Figs. 4a-d. SEM micrographs show a bright main crystalline phase embedded in a dark residual amorphous matrix. The SNS microstructure is similar to the two-phase

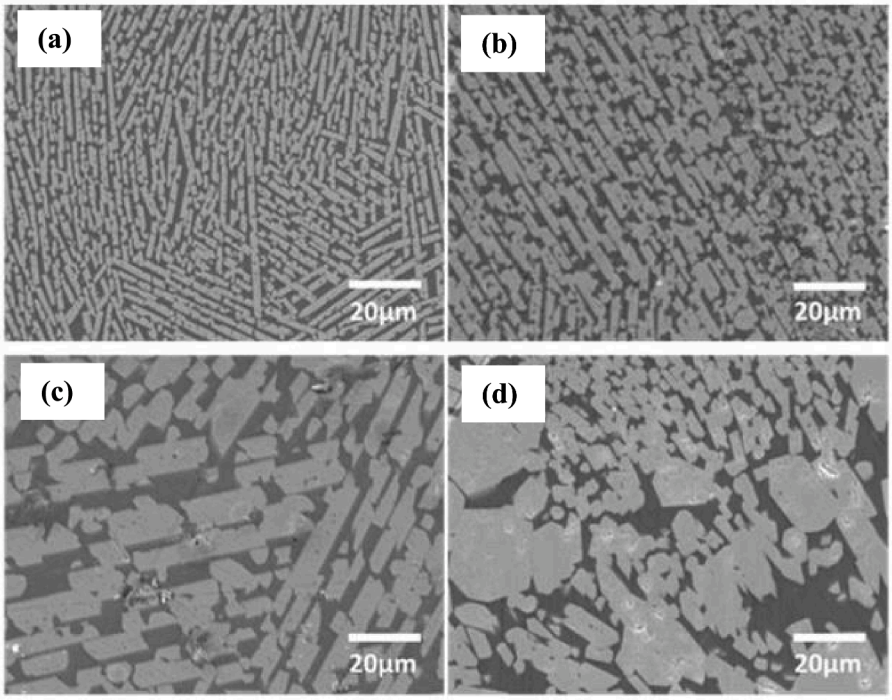

Fig. 4. SEM micrographs showing the microstructural evolution of the *heat-treated* SNS bulk samples devitrified at (a) 865 °C for 1 h (b) 865 °C for 5 h (c) 1050 °C for 1 h (d) 1050 °C for 5 h.

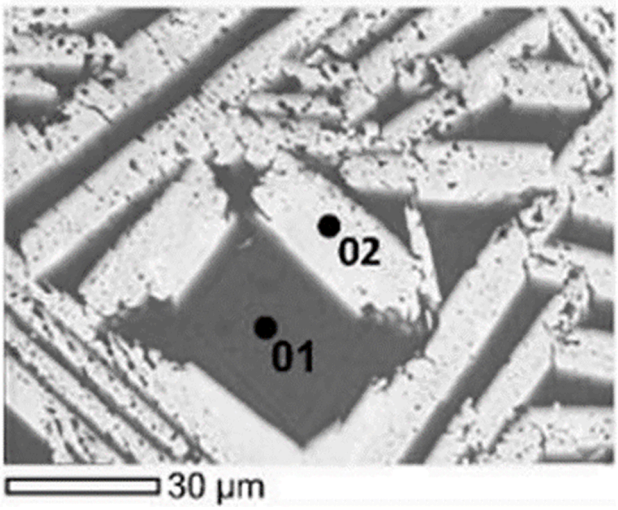

Tab. 1. EDX characterisation of SNS

	At. %	
Element	**Point 1**	**Point 2**
O	58.81	59.52
Na	14.39	0.61
Si	25.10	19.50
Sr	1.70	20.37

Fig. 5. *Heat-treated* SNS SEM image and EDS point analysis of the different phases.

microstructure displayed by Jee et al. [16], resulting from solid-state powder sintering (900 °C, 10 h). However, compared to this previous work, the microstructure shows some differences. Specifically, needle-like crystals are smaller than the large equiaxial crystals reported by Y. Jee et al. [16], especially for the samples subjected to lower treatment times and temperatures. Fig. 4a-c show the growth of the needle-like crystals resulting from the increasing process time and temperature. The heat treatment at 1050 °C for 5 h (Fig. 4d) led to a microstructure very similar to the previous results [16]. The most interesting aspect emerging from these results is the versatility of the melt quenching processing to accurately control the crystal sizes and shapes by tailoring the crystallisation treatment parameters (T,t). Such fine microstructure control indicates intense mass diffusive effects with fast elemental migration.

The related EDS elemental composition for the sample (Fig. 5) devitrified at 865 °C for 1 hour is shown in Table 1. The EDS analysis indicates that the crystalline phase (Point 2) has a very low concentration of Na (0.61 at.%), lower than the one reported previously and a higher content of Sr (20.37 at.%) and Si (19.50 at.%), thus indicating the

Table 1
EDX characterisation of SNS.

	At.%	
Element	Pount 1	Point 2
O	58.81	59.52
Na	14.39	0.61
Si	25.10	19.50
Sr	1.70	20.37

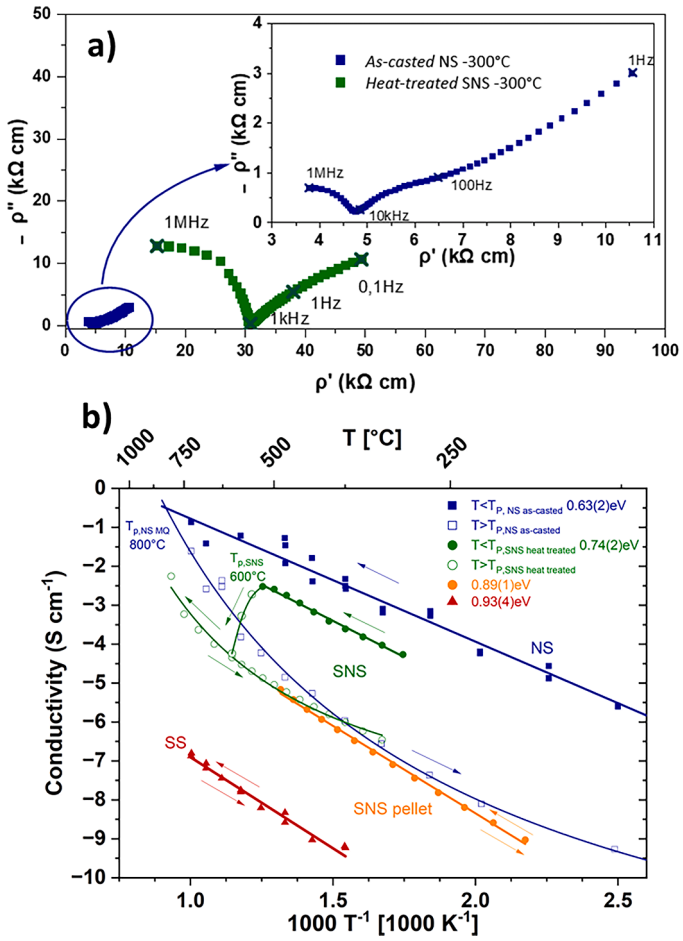

Fig. 6. Nyquist plot of the complex impedance at 300 °C of the heat-treated SNS and *as-casted* NS (a). Arrhenius plot of the ionic conductivities at different temperatures (b).

formation of SS as the main crystalline phase. The Na-rich (14.39 at.%) dark matrix (Point 1) can be attributed to an amorphous NS phase. These assumptions agree with data reported in the literature for the SNS system processed by a solid-state reaction technique [9–12,16]. SEM and EDS analyses show that the devitrification step leads to the crystallisation of $SrSiO_3$ during the heat treatment of the *as-casted* SNS bulk glass.

Electrochemical Impedance Spectroscopy was performed to study the electrical properties of the material. Fig. 6a shows the Nyquist plot for the heat-treated SNS and as-casted NS at 300 °C. The normalised NS resistivities are almost one order of magnitude lower than SNS, hence underlining that NS controls the conductivity, and the presence of SS decreases its magnitude.

The NS' lower resistivities are reflected in the higher conductivities (Fig. 6b). The conductivity measurements on NS are stable on the first three cycles (solid blue squares). Still, when the temperature is decreased from 750 °C (cooling third run), a conductivity drop appears (hollow blue squares). The conductivities calculated during the fourth run are stable and follow the results obtained during the cooling of the third run. The conductivities measured on the heat-treated SNS are comparable to the ones reported by Jee et al. [16]. Heat-treated SNS show a transition at 530 °C; a similar behaviour was shown by the conductivities of solid-state SNS [17]. NS shows higher conductivities than SNS, which is consistent with the results obtained by Jee et al., where samples produced with a solid-state technique were made. In solid-state NS, the conductivity drops at T >500 °C [17]. Instead, the stability window is wider for an as-casted bulk NS (Ag-electrode). The

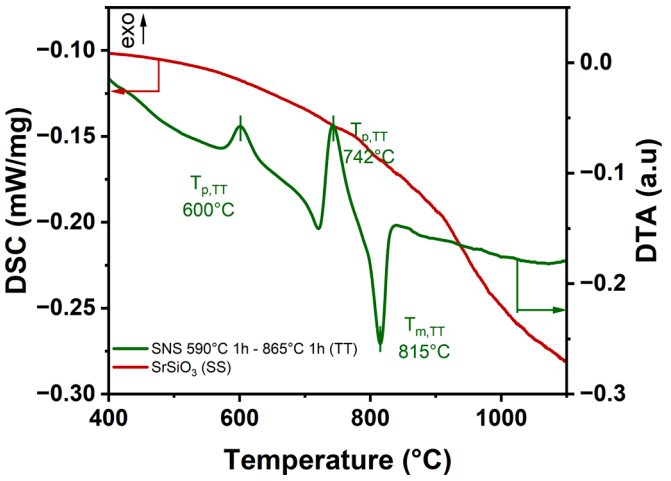

Fig. 7. DTA and DSC results on SS and SNS *heat-treated* samples.

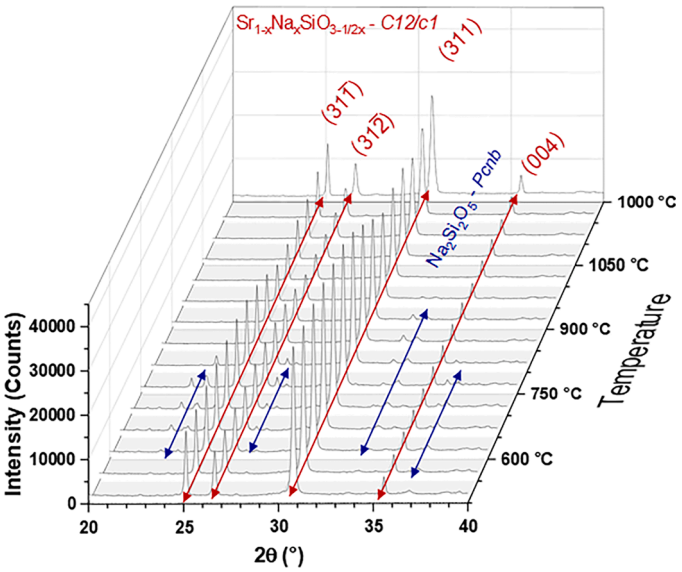

Fig. 8. In-situ XRD of the SNS *heat-treated* at 1050 °C.

NS conductivity drop is higher in the as-casted NS (750 °C) than in SNS. The result was confirmed in the DSC analysis (Fig 7). Fig. A.1 (Appendix) also shows the conductivities of the different SNS samples produced where no clear difference can be seen.

Therefore, we can assume that the nucleation of RC—NS in these cases is comparable even if the morphology of the samples differs. The reason for investigating the thermal behaviour under cycling (with heating and cooling) was to assess the nucleation and crystallisation process in the glassy matrix, thus demonstrating the different thermal treatment effects on affecting or restoring the conductivity.

Furthermore, Fig. 6b shows the results for the *heat-treated* SNS sample at 865 °C (1 hour) (Pt-electrodes). The *pellet* SNS (Pt-electrodes) and SS (Ag-electrodes) conductivities are also reported in Fig. 6b (orange circle and red triangle, respectively). The *pellet* conductivities are almost three orders lower than the melt-quenched sample. Since the conductivities lay in the same range as RC—NS and *heat-treated* SNS after recrystallisation's conductivities, the *pellet* samples likely underwent the same recrystallisation process during production. The SS conductivities are more than six orders of magnitude lower than the NS's. SS doesn't show any conductivity transition under thermal cycling. SS's conductivity is scarce, which explains the lower conductivity of SNS since the material acts as an insulator.

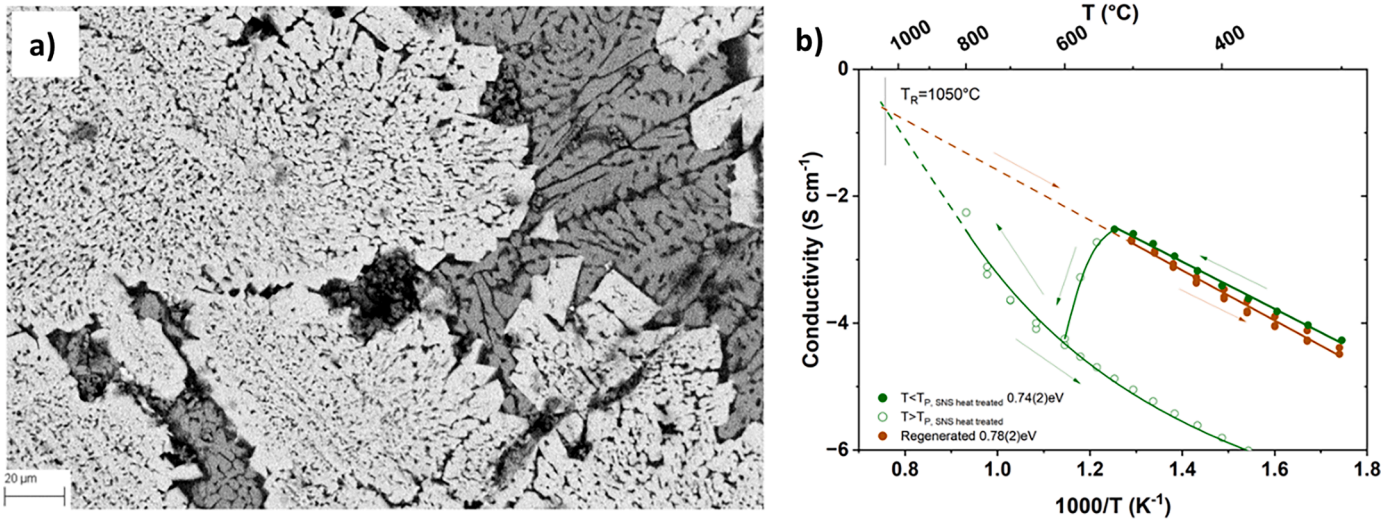

Fig. 9. Microstructure of the SNS regenerated at 1050 °C (a). Arrhenius plot of the ionic conductivities at different temperatures of the SNS regenerated sample compared to the pristine ionic conductivities of the heat-treated SNS sample (green points)(b).

The measurements in air and 3 % H_2/Ar on SNS, both *pellet* and *heat-treated* (865 °C), do not show any significant difference (Pt-electrodes) (Fig A.2, Appendix), as also reported in the literature, confirming the ionic nature of the conductivity [15]. These results confirm the hypothesis that the main conduction mechanism in the material is caused by the sodium ion and not by oxygen vacancies.

DTA measurements on NS have shown that the first recrystallisation process occurs at 800 °C (Fig. 2), consistent with the previous conductivity results. Different processes occur earlier in the SNS sample (Fig. 7), specifically at 600 and 742 °C. This effect suggests SS acts as a nucleation agent for RC—NS and causes earlier nucleation of this crystalline phase. As expected, the SS phase does not undergo any other phase transition in the same temperature range (Fig. 7). The $SrSiO_3$ phase is already present in the *heat-treated* sample material, as shown previously in Fig. 3. Therefore, the transitions occurring in SNS may be caused only by the NS, which recrystallises and causes the conductivity drop.

The SNS treated at 1050 °C phase temperature dependence was analysed via in-situ XRD (Fig. 8). The $SrSiO_3$ monoclinic structure with symmetry *C12/c1* is present. No other peaks are observed at room temperature (Fig. 3), thus indicating the presence of $SrSiO_3$ as the only crystalline phase constituting the sample. Upon heating, additional low-intensity diffraction peaks not matching with the $SrSiO_3$ main phase appear above 500 °C and significantly increase in intensity above 600 °C, thus indicating the formation of crystalline secondary phases expected from the DSC results. Most of the newly appeared minor peaks correspond to reflections of the $Na_2Si_2O_5$ orthorhombic phase with symmetry *Pcnb*. This result agrees with the results discussed previously and demonstrates the crystallisation of the amorphous $Na_2Si_2O_5$ when heated above its glass-transition temperature. This transformation is responsible for the conductivity drop in the SNS *heat-treated* sample shown in Fig. 6b. Additional peaks (*e.g.*, 26° and 32.9°) starting from 700 °C (Fig. A.3, Appendix) indicate the presence of other possible $Na_2Si_2O_5$ symmetries, like the *Pbc21*. The precise identification is difficult due to the limited reflections and low relative intensity. The formation of this additional phase is also supported by the exothermic event reported in Fig. 7, around 742 °C.

From the Rietveld Refinement of the multiple XRD patterns, an approximate fraction of $Na_2Si_2O_5$ of ≈ 20 % was estimated for temperatures between 650 °C and 800 °C [18]. In addition, the refinement indicated little to no Na^+ atomic occupation in the Sr^{2+} sites, suggesting limited Na incorporation into the $SrSiO_3$ phase by doping. This observation agrees with the limited compositional overlap observations for the Na and Sr EDS compositions (Table 1).

A further increase in temperature reveals the complete disappearance of crystalline $Na_2Si_2O_5$ above 900 °C (Fig. 8). In particular, for temperatures higher than 1000 °C, only reflections associated with the refractive and insulating *C12/c1* $SrSiO_3$ phase can be observed. During the cooling, no peaks associated with $Na_2Si_2O_5$ appear when crossing the crystallisation temperature range. The disappearance of the second phase can be associated with $Na_2Si_2O_5$ crystalline phase melting, which occurs above 815 °C, where a marked endothermic peak is observed in the DTA curve (Fig. 7). This agrees with the $Na_2Si_2O_5$-SiO_2 phase diagram [23] where a eutectic thermal event is reported around 810 °C. The NS melting was also seen in the DSC measurement of the melt-quenched NS (Fig. 2). In this case, the peak position temperature is slightly different, 870 °C, with an onset at 835 °C.

The bulk *heat-treated* sample previously subjected to a thermal treatment at 800 °C was heat treated up to 1050 °C. The corresponding DTA runs (Fig. 7), resulting from heating up to 1050 °C, show no further crystallisation peaks during heating. However, the endothermic peak corresponding to the melting of the sodium silicate is at about 815 °C, although no peaks are detectable in the DTA curve during cooling from 1050 °C. Thus it confirms that $Na_2Si_2O_5$ remain as an amorphous phase (glass)after heating above 1000 °C, as revealed by the XRD analysis.

The most striking consequence of heating the system above 1000 °C was restoring the original microstructure and conductivity completely. The EIS thermally cycled SNS *heat-treated* sample (865 °C for 1 h) was regenerated by a heat treatment at 1050 °C for 5 h. Fig. 9a shows the sample previously crystallised at 865 °C for 1 h, thermally cycled up to 800 °C, and partly regenerated at 1050 °C for 1 h. The microstructure is similar to the SNS heat treated at 1050 °C for 5 h; the sample shows a partially crystallised NS phase. The EIS analysis also highlights the results in the Arrhenius plots in Fig 9b (RT-500 °C, 50 °C step). The *heat-treated* sample after the transition is nearly completely regenerated after thermal treatment at 1050 °C. The regenerated amorphous NS phase restores the initial ionic conductivities (brown points), and operational conditions below 500 °C preserve the pristine ionic conductivity properties (green points in Fig. 9b). The *heat-treated* sample appeared dimensionally stable. This stability may be induced by the SS phase inside the material, which does not undergo any phase transition or melting. Instead, NS showed deformation at a temperature below its melting point (870 °C). A regeneration could not be done since the sample would deform, and the conductivities could not be restored. Regenerating materials are advantageous because they can heal damage and prolong their lifespan, lowering costs, increasing durability and reducing environmental impact.

4. Conclusions

The 31SrO-12.7Na2O-56.3SiO2 (SNS) composites and $Na_2Si_2O_5$ (NS) are promising candidates for All-Solid-State-Batteries electrolytes. We investigated how a melt-quenching technique affected the materials' microstructure, phase and conductivities. This technique allows us to produce a glassy amorphous $Na_2Si_2O_5$ and SNS composite, which showed interesting characteristics.

The fast-quenching process allows precise control of the microstructure without changing the electrical properties of the material. As previously reported for SNS composite, the amorphous $Na_2Si_2O_5$ controls the conductivity, and its crystalline phase insulates, impairing the conductivity. Thus, the fast-quenching, suppressing crystallisation, promotes ionic conductivity. We also show that the temperature stability range of amorphous $Na_2Si_2O_5$ is affected by the presence of $SrSiO_3$. The $Na_2Si_2O_5$ glass crystallises at lower temperatures if the $SrSiO_3$ crystalline phase is present due to probable heterogeneous nucleation. For the SNS, the conductivity gradually drops due to the incipient nucleation of recrystallised-$Na_2Si_2O_5$ at 530 °C, drastically reducing the percolative ionic transport in the presence of the multiple insulating phases, *i.e.*, $SrSiO_3$ and the crystalline $Na_2Si_2O_5$.

For the individual amorphous $Na_2Si_2O_5$, the conductivities in the RT-500 °C are similar to the one reported in the literature. However, the stability range is now clarified. The glassy $Na_2Si_2O_5$ is stable in a wide temperature range, and we reached a high conductivity of 10^{-1} S cm^{-1} at 750 °C. When purified from the $SrSiO_3$ phase, the material showed a full crystallisation peak at 800 °C. The material also shows good conductivity and stability, is largely available, and the production technology is scalable. Thus, amorphous $Na_2Si_2O_5$ can be a candidate for an intermediate-temperature Na-ion all-solid-state battery electrolyte. On the other hand, the presence of a crystalline phase increases the thermal-mechanical properties of the final composite. The strontium silicate phase allows regeneration of the composite at 1050 °C, and the resulting conductivities are fully restored in a range of operational conditions below 500 °C.

Declaration of Competing Interest

The authors declare no conflict of interest.

Acknowledgements

Vincenzo Esposito, Jun Zhang, Alessandro Palliotto, and Victor Burrato Tinti would like to acknowledge the Indipendent Research Fund Denmark -Technology And Production (DFF-Research Project 2, NEMO 1032–00261B).

Appendices A

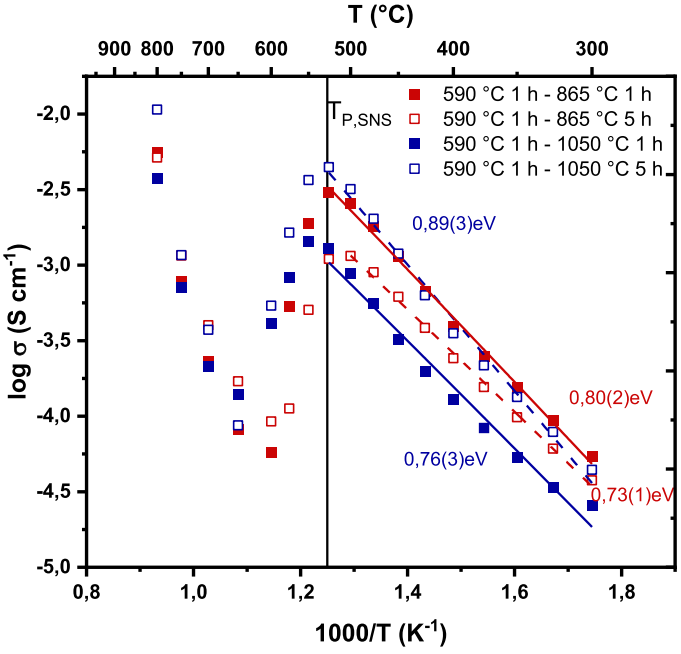

Fig. A.1. Arrhenius plot of the samples treated at 590 °C for 1 hour and treated at 865 °C and 1050 °C, red and blue, respectively, for 1 hour (Solid) and 5 h (Hollow) (Pt-electrodes).

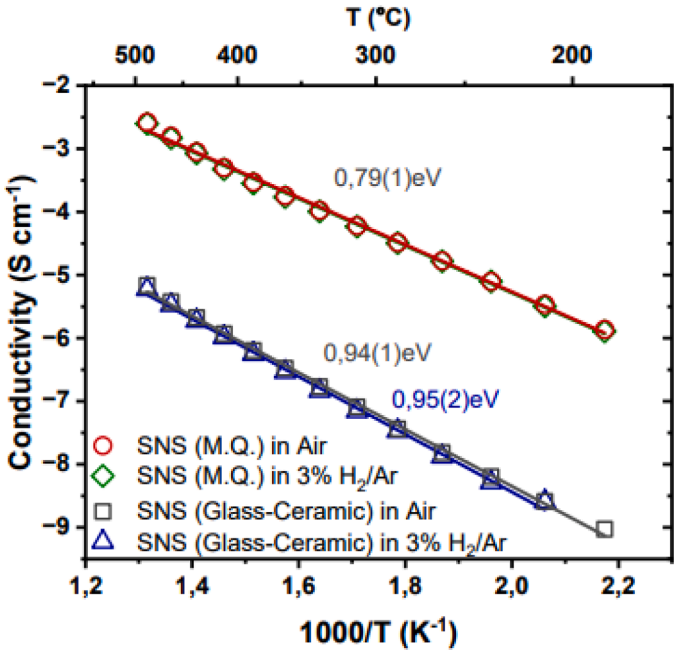

Fig. A.2. Arrhenius plot of the pellet sample in air (blue triangle) or 3 % H_2/Ar (black square). Conductivities measured on the heat-treated sample, measured in air (red circle) or in 3 % H_2/Ar (green rhombus) (Pt-electrodes).

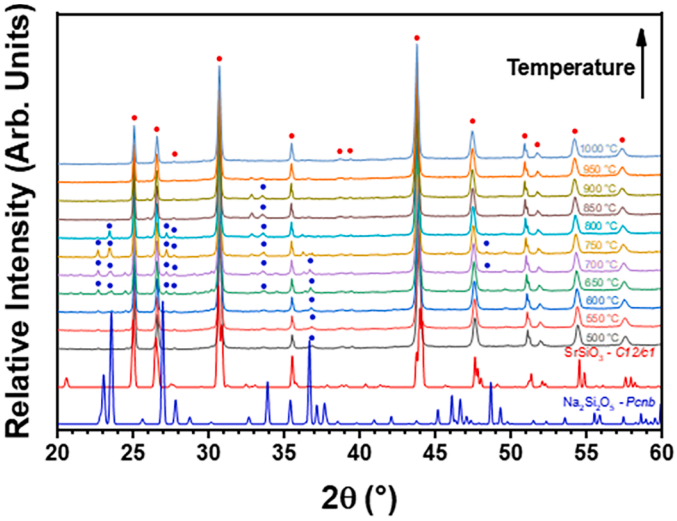

Fig. A.3. In-situ XRD results of the fast-quenched SNS from 500 °C to 1000 °C. In red the peaks are assigned to SS and in blue to NS.

References

[1] P.M. Gonzalez Puente, S. Song, S. Cao, L.Z. Rannalter, Z. Pan, X. Xiang, Q. Shen, F. Chen, Garnet-type solid electrolyte: advances of ionic transport performance and its application in all-solid-state batteries, J. Adv. Ceram. 10 (5) (2021) 933–972.

[2] H. Wu, D. Zhuo, D. Kong, Y. Cui, Improving battery safety by early detection of internal shorting with a bifunctional separator, Nat. Commun. 5 (1) (2014) 5193.

[3] W. Zhang, F. Zhang, F. Ming, H.N. Alshareef, Sodium-ion battery anodes: status and future trends, EnergyChem 1 (2) (2019), 100012.

[4] H. Che, S. Chen, Y. Xie, H. Wang, K. Amine, X.Z. Liao, Z.F Ma, Electrolyte design strategies and research progress for room-temperature sodium-ion batteries, Energy Environ. Sci. 10 (5) (2017) 1075–1101.

[5] C. Delmas, Sodium and sodium-ion batteries: 50 years of research, Adv. Energy Mater. 8 (17) (2018), 1703137.

[6] S. Gandi, V.S. Chidambara Swamy Vaddadi, S.S. Sripada Panda, N.K. Goona, S. R. Parne, M. Lakavat, A Bhaumik, Recent progress in the development of glass and glass-ceramic cathode/solid electrolyte materials for next-generation high capacity all-solid-state sodium-ion batteries: a review, J. Power Sources 521 (2022), 230930.

[7] P. Singh, J.B. Goodenough, Monoclinic $Sr_{1-x}Na_xSiO_{3-0.5x}$: new superior oxide ion electrolytes, J. Am. Chem. Soc. 135 (27) (2013) 10149–10154.

[8] R.D. Bayliss, S.N. Cook, D.O. Scanlon, S. Fearn, J. Cabana, C. Greaves, J.A. Kilner, S.J. Skinner, Understanding the defect chemistry of alkali metal strontium silicate solid solutions: insights from experiment and theory, J. Mater. Chem. A 2 (42) (2014) 17919–17924.

[9] I.R. Evans, J.S.O. Evans, H.G. Davies, A.R. Haworth, M.L. Tate, On $Sr_{1-x}Na_xSiO_{3-0.5x}$ new superior fast ion conductors, Chem. Mater. 26 (18) (2014) 5187–5189.

[10] K.K. Inglis, J.P. Corley, P. Florian, J. Cabana, R.D. Bayliss, F. Blanc, Structure and sodium ion dynamics in sodium strontium silicate investigated by multinuclear solid-state NMR, Chem. Mater. 28 (11) (2016) 3850–3861.

[11] A.C. Kundur, M.P. Singh, V.A. Sethuraman, Sodium doped strontium silicates as electrolyte for intermediate temperature solid oxide fuel cells, ECS Trans. 78 (1) (2017) 467–475.

[12] C. Tealdi, L. Malavasi, I. Uda, C. Ferrara, V. Berbenni, P. Mustarelli, Nature of conductivity in $SrSiO_3$-based fast ion conductors, Chem. Commun. 50 (94) (2014) 14732–14735.

[13] R.D. Bayliss, S.N. Cook, S. Fearn, J.A. Kilner, C. Greaves, S.J. Skinner, On the oxide ion conductivity of potassium doped strontium silicates, Energy Environ Sci 7 (9) (2014) 2999.

[14] P. Singh, J.B. Goodenough, Sr1−xKxSi1−yGeyO3−0.5x: a new family of superior oxide-ion conductors, Energy Environ. Sci. 5 (11) (2012) 9626.

[15] Y. Jee, P.H. Chien, E. Villarreal, Y.Y. Hu, K. Huang, Crystallisation of amorphous Na2Si2O5 as a Na-ion conductor, Solid State Ion. 296 (2016) 63–70.
[16] Y. Jee, X. Zhao, K. Huang, On the cause of conductivity degradation in sodium strontium silicate ionic conductor, Chem. Commun. 51 (47) (2015) 9640–9642.
[17] Y. Jee, X. Zhao, X. Lei, K. Huang, Phase Relationship and ionic conductivity in Na–$SrSiO_3$ ionic conductor, J. Am. Ceram. Soc. 99 (1) (2016) 324–331.
[18] H.M. Rietveld, A profile refinement method for nuclear and magnetic structures, J. Appl. Crystallogr. 2 (2) (1969) 65–71.
[19] A.A. Coelho, *TOPAS* and *TOPAS-Academic* : an optimisation program integrating computer algebra and crystallographic objects written in C++, J. Appl. Crystallogr. 51 (1) (2018) 210–218.
[20] E. Dinnebier, Robert, Andreas Leineweber, John S.O. Evans, Rietveld Refinement: Practical Powder Diffraction Pattern Analysis using TOPAS, De Gruyter, Berlin, Boston, 2018.
[21] A.K. Pant, D.W.J. Cruickshank, The crystal structure of α-Na2Si2O5, Acta Crystallogr. Sect B Struct. Crystallogr. Cryst. Chem. 24 (1) (1968) 13–19.
[22] M.E. Fleet, G.S. Henderson, Epsilon sodium disilicate: a high-pressure layer structure [$Na_2Si_2O_5$], J. Solid State Chem. 119 (2) (1995) 400–404.
[23] J. Williamson, F.P. Glasser, Phase Relations in the System $Na_2Si_2O_5$ -SiO_2, Science 148 (3677) (1965) 1589–1591.
[24] L. Lin, W. Guo, M. Li, J. Qing, C. Cai, P. Yi, Q. Deng, W. Chen, Progress and perspective of glass-ceramic solid-state electrolytes for lithium batteries, Materials 16 (7) (2023) 2655 (Basel).
[25] Q. Ma, F. Tietz, Solid-state electrolyte materials for sodium batteries: towards practical applications, ChemElectroChem 7 (13) (2020) 2693–2713.
[26] R. Martinez-Coronado, P. Singh, J. Alonso-Alonso, J.B Goodenough, Structural investigation of the oxide-ion electrolyte with $SrMO_3$ (M = Si/Ge) structure, J. Mater. Chem. A 2 (12) (2014) 4355–4360.
[27] T.K. Pietrzak, M. Wasiucionek, J.E. Garbarczyk, Towards higher electric conductivity and wider phase stability range via nanostructured glass-ceramics processing, Nanomaterials 11 (2021) 1321.